

# Peculiar emission from the new VHE gamma-ray source H1722+119

T. Terzić<sup>1</sup>, A. Stamerra<sup>2</sup>, the MAGIC Collaboration, F. D'Ammando<sup>3,4</sup> (for the Fermi-LAT Collaboration), C. M. Raiteri<sup>5</sup>, M. Villata<sup>6</sup>, F. Verrecchia<sup>6,7</sup>, T. Hovatta<sup>8,9</sup>, W. Max-Moerbeck<sup>10</sup>, A. C. S. Readhead<sup>11</sup>, R. Reinthal<sup>11</sup>, A. Berdyugin<sup>11</sup>, J. L. Richards<sup>12</sup>, O. Kurtanidze<sup>13</sup>

## ABSTRACT

The BL Lac object H1722+119 was observed in the very-high energy band (VHE,  $E > 100$  GeV) by the MAGIC (Major Atmospheric Gamma-ray Imaging Cherenkov) telescopes between 2013 May 17 and 22, following a state of high activity in the optical band measured by the KVA (Kungliga Vetenskapsakademien) telescope. Integrating 12.5 h of observation, the source was detected with a statistical significance of 5.9 sigma, with measured flux of  $f = (6.3 \pm 1.6) \times 10^{-12}$  ph cm<sup>-2</sup> s<sup>-1</sup> above 150 GeV, corresponding to  $(2.0 \pm 0.5)$  per cent of the Crab Nebula flux in the same energy range.

Contemporaneous observations were performed by the LAT (Large Area Telescope) on board the Fermi satellite in the high energy range (HE,  $100$  MeV  $< E < 100$  GeV), by instruments on board the Swift satellite in the UV and X-ray region and by the OVRO (Owens Valley Radio Observatory) telescope in the radio band, allowing us to build a quasi simultaneous multi-wavelength SED (spectral energy distribution). An unexpected feature in the  $\sim 3 \times 10^{14} - 10^{18}$  Hz frequency range of the SED was identified. A possible explanation using an inhomogeneous helical jet synchrotron self-Compton model is suggested.

The combination of HE and VHE gamma-ray observations, and the expected imprint of the extragalactic background absorption, allowed us to set a constraint on the redshift of this blazar to be  $z = 0.34 \pm 0.15$ .

No significant temporal variability of the flux in the HE and VHE bands was found. Contemporaneous data from the KVA and the OVRO telescopes show variable flux in optical and radio wavebands, respectively, although with different patterns.



## Multi wavelength light curve

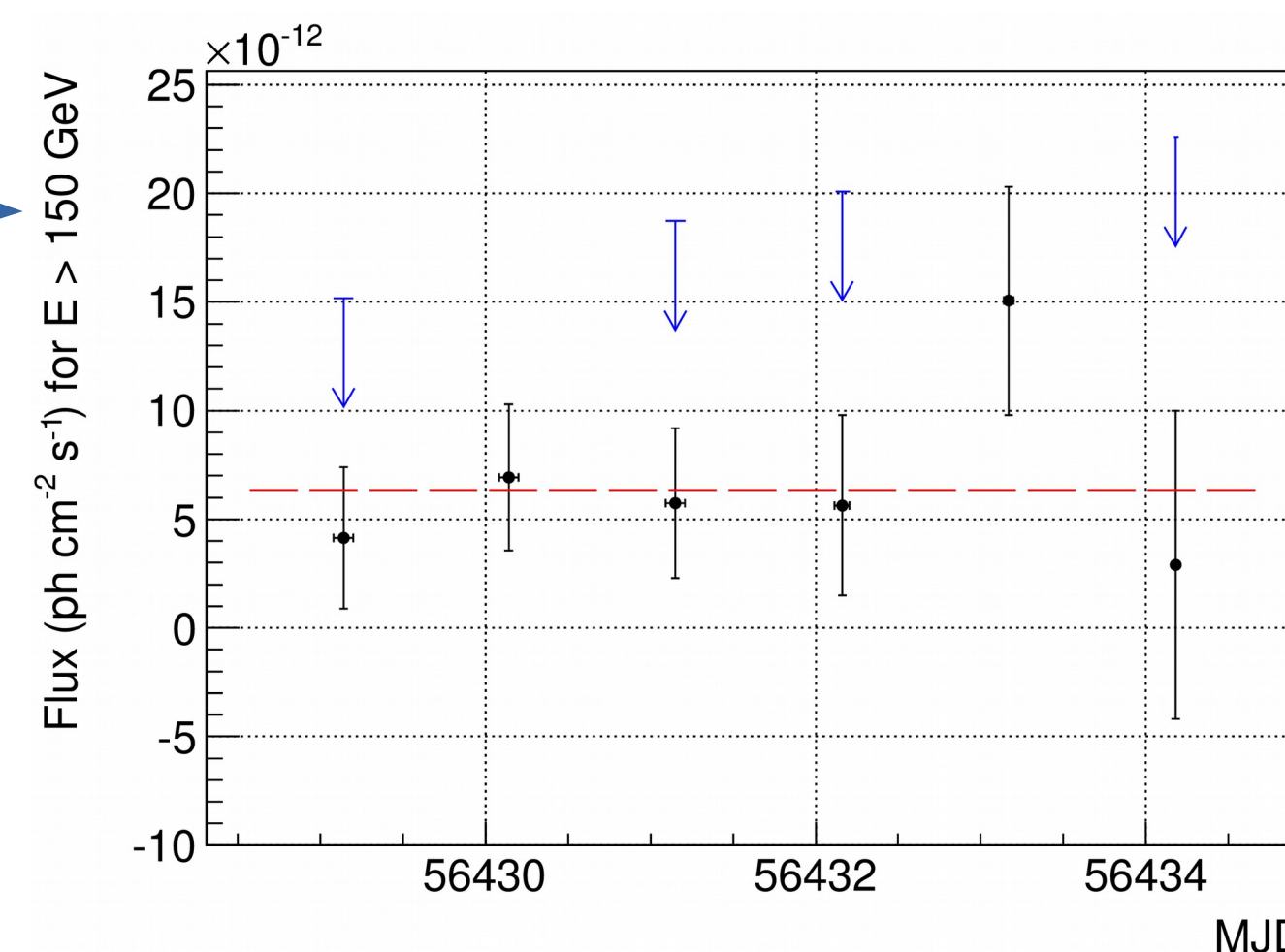
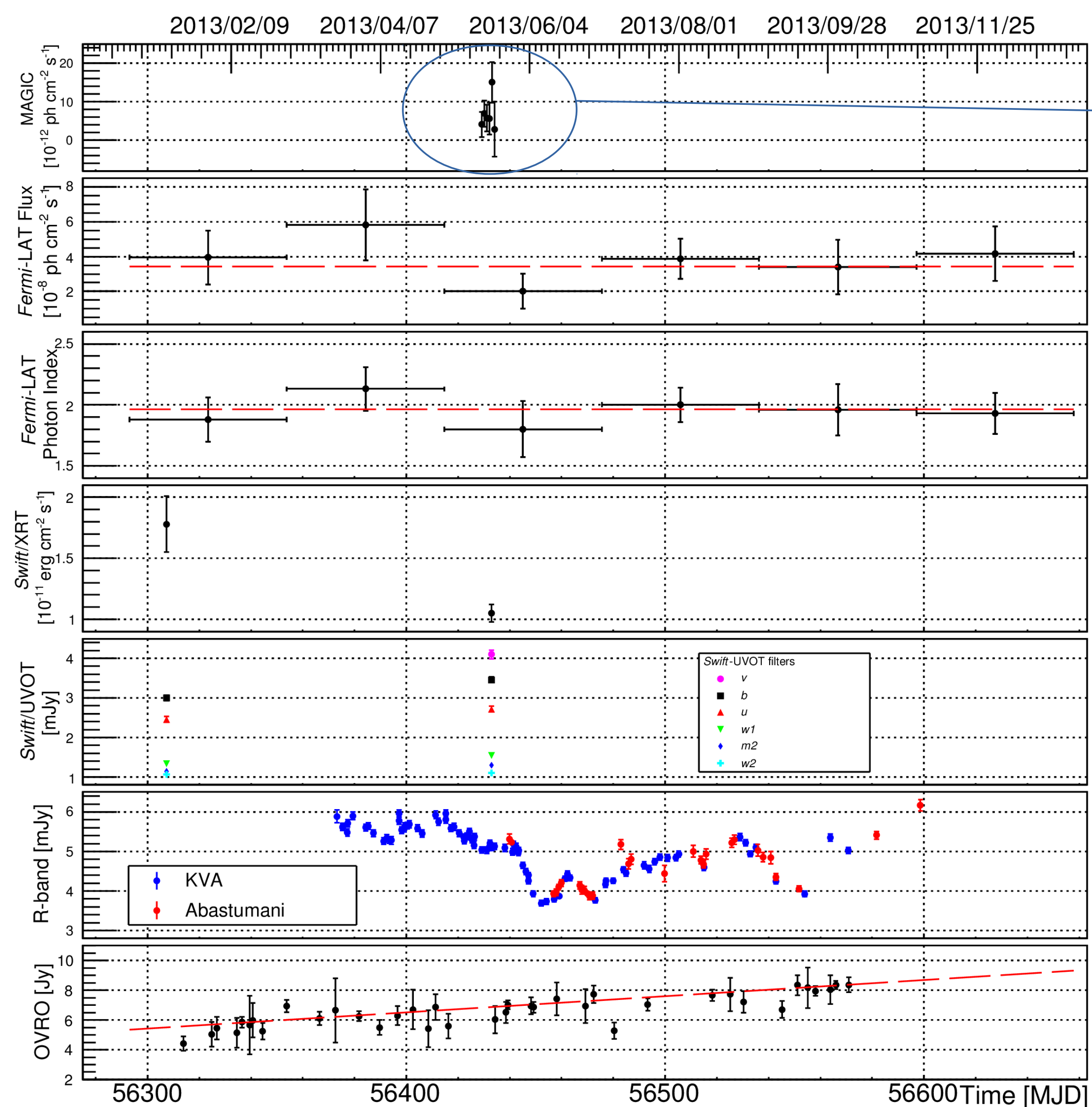


**Figure 1.** Light curve of H1722+119 for data collected during 2013. **Left:** Multiwavelength light curve during 2013. The data were collected (from top to bottom) by MAGIC ( $E > 150$  GeV), Fermi-LAT ( $0.1$  GeV  $< E < 100$  GeV), Swift/XRT, Swift/UVOT, KVA and Abastumani (R-band) and OVRO (15 GHz). The HE  $\gamma$ -ray light curve and the evolution of the spectral index, as measured by Fermi-LAT, are shown in 2-month time bins, while daily observations time-scale is used in the light curves in the other energy bands. Horizontal dashed lines in LAT panels represent the fit with a constant. The dashed line in the OVRO panel represents a linear function fit. **Above:** MAGIC nightly light curve for energies above 150 GeV. Horizontal error bars represent the duration of each observation. Vertical arrows represent ULs for points whose relative error of the excess is  $> 0.5$ . The horizontal dashed line is a constant flux fit. **Fit parameters**  
MAGIC:  $f = (6.3 \pm 1.6) \times 10^{-12}$  ph cm<sup>-2</sup> s<sup>-1</sup> - equivalent to  $2.0 \pm 0.5$  of the Crab Nebula flux above 150 GeV;  $\chi^2 / \text{NDF} = 3.5/5$   
Fermi-LAT:  $f = (3.4 \pm 0.6) \times 10^{-8}$  ph cm<sup>-2</sup> s<sup>-1</sup>;  $\chi^2 / \text{NDF} = 3.9/5$   
Fermi-LAT: spectral index =  $1.96 \pm 0.07$ ;  $\chi^2 / \text{NDF} = 1.7/5$   
OVRO:  $p_0 = (5.2 \pm 0.2) \times 10^{-2}$  Jy,  $p_1 = (1.07 \pm 0.10) \times 10^{-4}$  Jy/day;  
 $\chi^2 / \text{NDF} = 39.68/36$  (F [Jy]) =  $p_0 + p_1 \times (t - 56300)$ [MJD]

## FACILITIES

- MAGIC (Major Atmospheric Gamma-Ray Imaging Cherenkov):  $E > 50$  GeV [1 - 4]
- Fermi-LAT (Large Area Telescope):  $20$  MeV  $< E < 300$  GeV [5, 6]
- Swift-XRT:  $200$  eV  $< E < 10$  keV [7]
- Swift-UVOT:  $170$  nm  $< \lambda < 600$  nm [8]
- KVA (Kungliga Vetenskapsakademien) telescope: R-band [9, 10]
- Abastumani: R-band [11]
- OVRO (Owens Valley Radio Observatory):  $15$  GHz [12]

## REDSHIFT

### Redshift from optical observations

- featureless optical spectrum [15]
- absorption feature  $\rightarrow z = 0.018$  [16]
- no intrinsic features in the optical spectra  $\rightarrow z > 0.17$  [17]
- host galaxy not detected  $\rightarrow z > 0.4$  [Farina et al. (2013, priv. comm.)]
- no intrinsic or intervening spectral lines  $\rightarrow z > 0.35$  [14]

### Redshift from HE/VHE band

- VHE  $\gamma$ -rays interact with the extragalactic background light (EBL)
- the VHE flux attenuation depends on the redshift of the source and energy of  $\gamma$ -rays
- assuming:
  - HE and VHE  $\gamma$ -rays are created by the same physical processes in the same region
  - the intrinsic spectrum in the VHE range cannot be harder than the spectrum in the HE range
- methods:
  - redshift at which VHE and HE spectral slopes match [18]  $\rightarrow z = 0.34 \pm 0.15_{\text{stat}} \pm 0.05_{\text{meth}}$ ; UL:  $z < 1.06$  (95% C.L.)
  - redshift at which de-absorbed spectrum shape becomes parabolic in a  $\log(dN/dE)$  vs  $\log E$  representation [19]  $\rightarrow$  UL:  $z < 0.95$

## Spectral energy distribution

**Figure 2 (right).** The H1722+119 SED. Blue circles represent data contemporaneous to MAGIC observations. The MAGIC measured data are shown by empty blue squares, while full blue squares indicate the de-absorbed points for  $z = 0.4$  using the EBL model from [13]. Fermi-LAT data are shown by circles, while arrows represent Fermi-LAT ULs. The Swift data indicated by blue circles were taken on 2013 May 20 (MJD 56432). The KVA R-band point represented by a blue circle was taken on the same night. The OVRO measurement represented by a blue circle was taken on 2013 May 22 (MJD 56434). Red triangles show the Swift data from 2008 May 31 (MJD 54617). The green solid line in the  $10^{14} - 10^{15}$  Hz range indicates data from [14], but they were not considered for the fit. Archival data from 2MASS and WISE are shown by empty grey circles, and were not considered for the fit. The blue long-dashed line indicates the fit of the helical jet model to the 2013 data, while the fit to the 2008 data is indicated by the red dash-dot line. Both models represent the intrinsic VHE emission. Only blue and red points were considered for modelling.

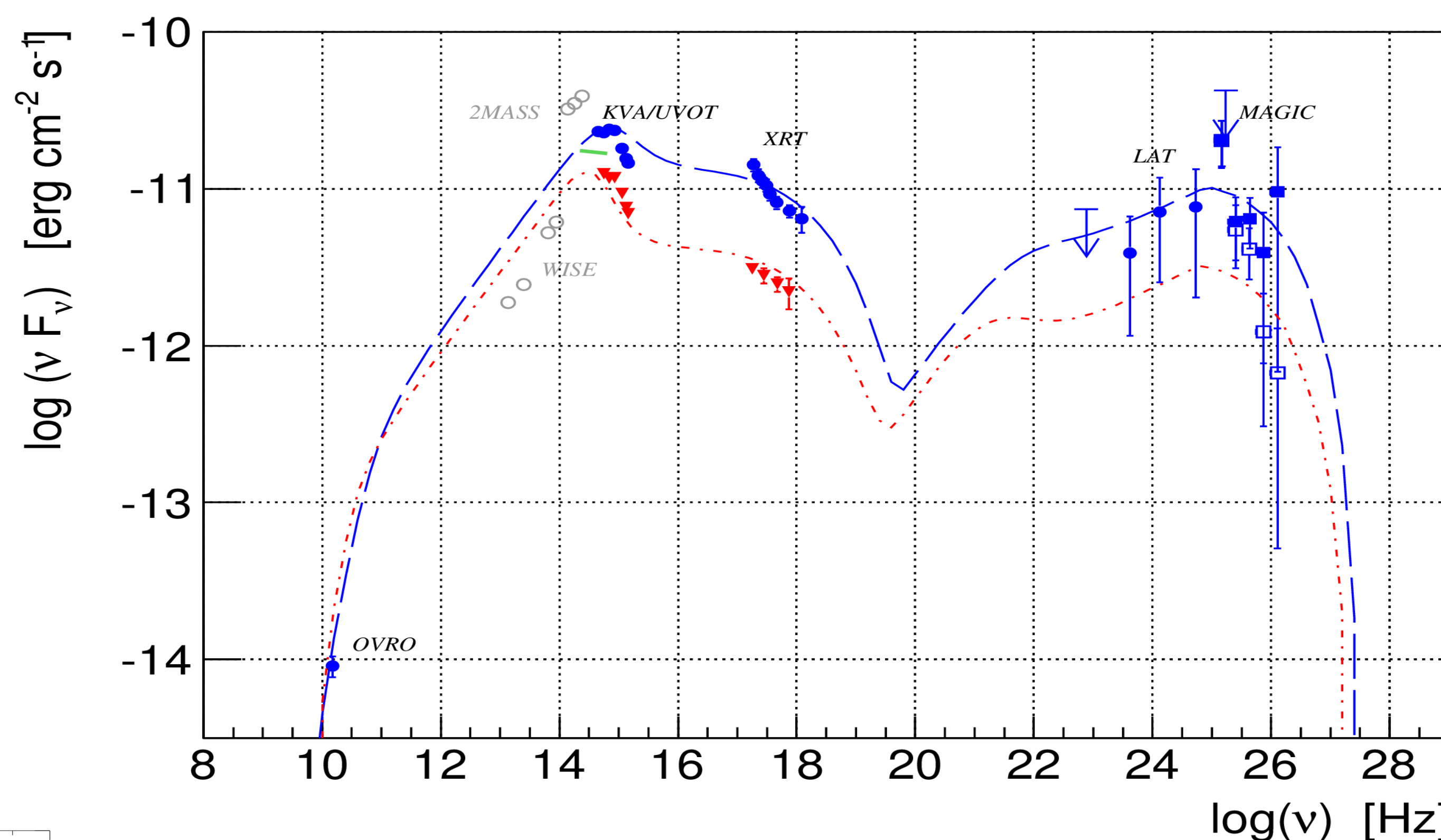
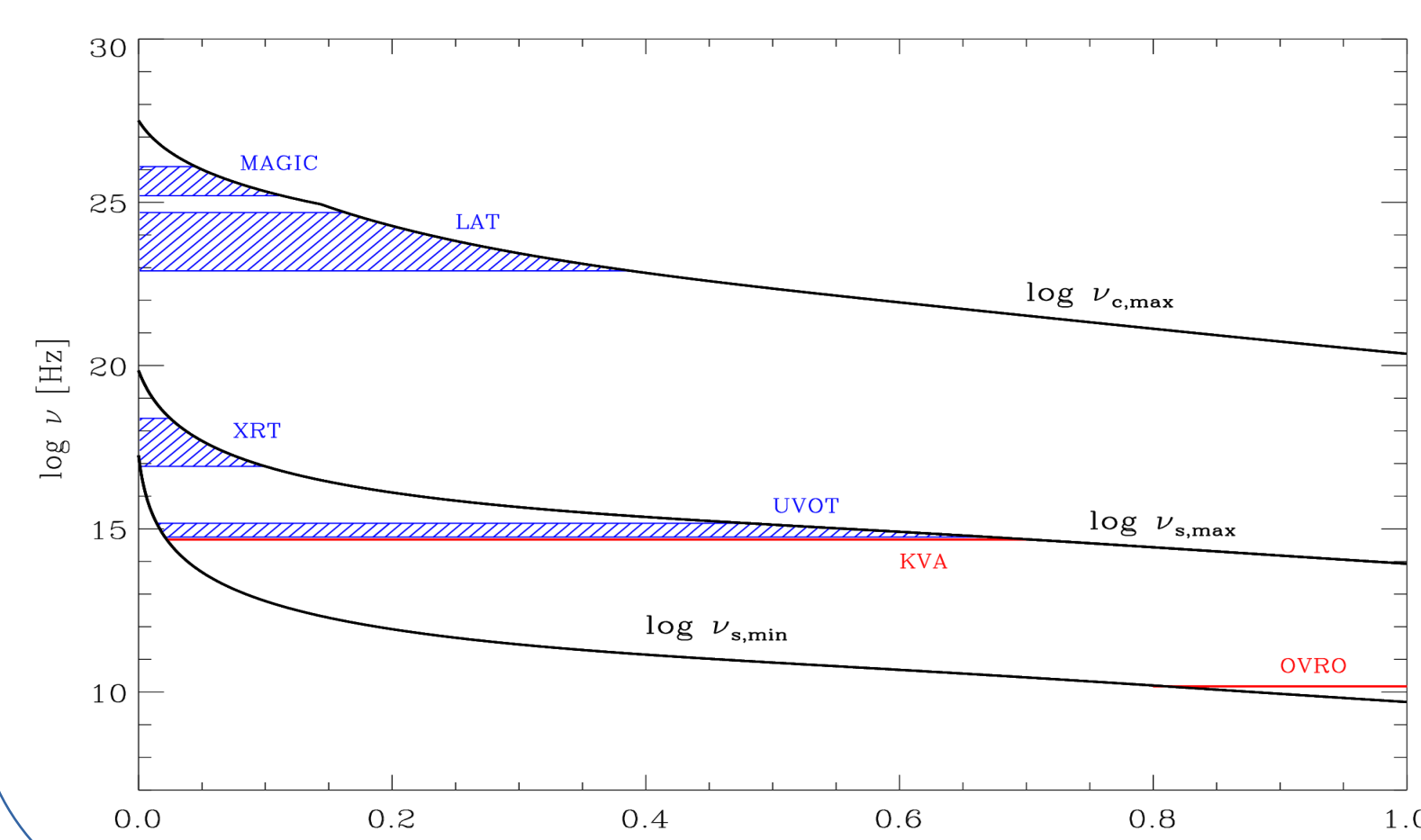


**Figure 3 (below).** The trend of the observed frequencies as a function of the distance along the helical jet axis  $z$  (whose unit length can be estimated to be about 0.1 pc). The location of the regions that contribute to the emission observed by the various instruments is highlighted. The plot refers to the high emission state shown in the SED plot.



### SED peculiarity

- optical-UV spectrum curved, with a peak in the  $b$  band and a steep slope in the UV
- no evidence of emission at any frequency from the accretion disc, dust torus or BLR
- the ratio of beamed to thermal emission set to be  $\geq 400$  by [14]
- the estimated redshift, and the upper limits set by [14] rule out the possibility that the feature is due to the inset of the Lyman limit
- the connection between optical-UV and the X-ray bands requires an inflection point, which is unexpected if both the optical-UV and X-ray emissions are produced by a synchrotron process in the same jet region

### Helical jet model

- Based on the idea that the emitting jet has a helical structure with a pitch angle  $\zeta$ . The helix axis is assumed to be along  $z$  and  $\psi$  is the angle defined by the axis with the line of sight. The jet viewing angle varies along the helical path as

$$\cos \theta(z) = \cos \psi \cos \zeta + \sin \psi \sin \zeta \cos(\phi - az)$$

where  $\phi$  is the azimuthal difference between the line of sight and the initial direction of the helical path, and  $a$  defines the azimuthal angle  $\phi = az$ .

- The jet is inhomogeneous since each slice of the jet can radiate, in the plasma rest reference frame, synchrotron photons between a minimum and a maximum frequency, both of which decrease along the jet. Hence, the X-ray radiation comes from the inner part of the emitting jet, while radio photons are produced downstream.
- High-energy photons are obtained by inverse-Compton scattering of the synchrotron photons by the same relativistic electrons emitting them (synchrotron self-Compton, i.e. SSC) in each portion of the jet emitting synchrotron radiation. The electron Lorentz factor also decreases along the jet.
- The observed flux density has a power law dependence on the frequency and a cubic dependence on the Doppler beaming factor.
- The variation of the viewing angle  $\theta$  along the helical path implies a change of the beaming factor so that the flux at a given frequency peaks when the jet region mostly contributing to it has minimum  $\theta$ . Hence, the model predicts observed flux variations due to geometrical effects, even if the intrinsic flux remains constant.
- The emissivity varies along the jet as shown in Figure 3.
- The helical jet model solves the problem of the optical-UV to X-ray discontinuity.
- Both SED fits are obtained with the same choice of model parameters, with the exception of the angle  $\phi$ , which changes from 25 to 31 deg when going from the high to the low state. This underlines how variations of a few degrees in the viewing angle alone may take account of the observed flux changes.
- Details on the helical jet model can be found in [20, 21].

## MAIN RESULTS

- VHE signal detected for the first time with significance of 5.9  $\sigma$
- redshift estimated to:  $z = 0.34 \pm 0.15_{\text{stat}} \pm 0.05_{\text{meth}}$  ( $z_{\text{UL}} = 0.95$ )
- steady flux in HE and VHE ranges
- indication of spectral hardening at HE in 2013 May
- significant flux variations in optical and radio bands
- no indication of connection between different energy bands
- interesting feature in the optical-UV band
- emission can be explained with the helical jet model from [20]

## REFERENCES

- [1] Aleksić J., et al., 2016, *Astroparticle Physics*, 72, 61
- [2] Aleksić J., et al., 2016, *Astroparticle Physics*, 72, 76
- [3] Lombardi S., et al., 2011, *ICRC32*, 3, 266
- [4] Zanin R., et al., 2013, *ICRC33*
- [5] Atwood W. B., et al., 2009, *ApJ*, 697, 1071
- [6] Ackermann M., et al., 2012, *ApJS*, 203, 4
- [7] Burrows D. N., et al., 2005, *Space Sci. Rev.*, 120, 165
- [8] Roming P., et al., 2005, *Space Sci. Rev.*, 120, 95
- [9] <http://users.utu.fi/kani/1m>
- [10] Nilsson et al. (2016, in prep.)
- [11] [http://www.oato.inaf.it/blazars/web/aba\\_info.html](http://www.oato.inaf.it/blazars/web/aba_info.html)
- [12] Richards J. L., et al., 2011, *ApJS*, 194, 29
- [13] Franceschini A., Rodighiero G., Vaccari M., 2008, *A&A*, 487, 837
- [14] Landoni M., et al., 2014, *A&A*, 570, A126
- [15] Brissenden R. J. V., et al., 1990, *ApJS*, 350, 578
- [16] Griffiths R. E., et al., 1989, *MNRAS*, 240, 33
- [17] Sbarufatti B., et al., 2006, *AJ*, 132, 1
- [18] Prandini E., et al., 2010, *MNRAS*, 405, L76
- [19] Mazin D., Goebel F., 2007, *ApJ*, 655, L13
- [20] Villata M., Raiteri C. M., 1999, *A&A*, 347, 30
- [21] Ahnen M. L., et al., 2016, *MNRAS*, 459, 3271

## AFFILIATIONS

- <sup>1</sup>University of Rijeka, HR-51000 Rijeka, Croatia, tterzic@phy.uniri.hr
- <sup>2</sup>INAF - National Institute for Astrophysics, I-00136 Rome, Italy
- <sup>3</sup>Dip. Di Fisica e Astronomia, Università degli Studi di Bologna, I-40127 Bologna, Italy
- <sup>4</sup>INAF - Istituto di Radioastronomia, I-40129 Bologna, Italy
- <sup>5</sup>INAF - Osservatorio Astronomico di Torino, I-10025 Pino Torinese (TO), Italy
- <sup>6</sup>INAF - Osservatorio Astronomico di Roma, I-00040 Monteporzio Catone, Italy
- <sup>7</sup>ASI Science Data Center (ASDC), I-00133 Roma, Italy
- <sup>8</sup>Aalto University Metsähovi Radio Observatory, Metsähovintie 114, FI-02540 Kylmäla, Finland
- <sup>9</sup>Cahill Center for Astronomy and Astrophysics, California Institute of Technology, Pasadena, CA 91125, USA
- <sup>10</sup>National Radio Astronomy Observatory (NRAO), PO Box 0, Socorro, NM 87801, USA
- <sup>11</sup>Tuorla Observatory, Department of Physics and Astronomy, University of Turku, Finland
- <sup>12</sup>Department of Physics, Purdue University, West Lafayette, IN 47907, USA
- <sup>13</sup>Abastumani Observatory, Mt. Kanobili, 0301 Abastumani, Georgia